Journal of Materials Chemistry

Cite this: J. Mater. Chem., 2012, 22, 9632

www.rsc.org/materials

PAPER

Cu,Zn,Al layered double hydroxides as precursors for copper catalysts in methanol steam reforming – pH-controlled synthesis by microemulsion technique†

Stefanie Kühl,[a] Matthias Friedrich,[b] Marc Armbrüster[b] and Malte Behrens*[a]

Received 24th November 2011, Accepted 14th March 2012
DOI: 10.1039/c2jm16138a

By co-precipitation inside microemulsion droplets a Cu-based catalyst precursor was prepared with a Cu : Zn : Al ratio of 50 : 17 : 33. A pH-controlled synthesis was applied by simultaneous dosing of metal solution and precipitation agent. This technique allows for continuous operation of the synthesis and enables easy and feasible up-scaling. For comparison conventional co-precipitation was applied with the same composition. Both techniques resulted in phase pure layered double hydroxide precursors and finally (after calcination and reduction) in small Cu nanoparticles (8 nm) and $ZnAl_2O_4$. By applying the microemulsion technique smaller $Cu/ZnAl_2O_4$ aggregates with less embedded Cu particles were obtained. The microemulsion product exhibited a higher BET and specific Cu surface area and also a higher absolute catalytic activity in methanol steam reforming. However, the Cu surface area-normalized, intrinsic activity was lower. This observation was related to differences in interactions of Cu metal and oxide phase.

1 Introduction

The well known $Cu/ZnO/Al_2O_3$ catalysts which are used for different industrial syntheses, like methanol synthesis, are obtained by co-precipitation, followed by calcination and reduction. Most active catalysts are prepared from zincian malachite precursors.[1,2] If aluminium is present in significant amounts (industrially applied Cu : Zn : Al composition: ≈60 : 30 : 10), the ternary hydrotalcite (layered double hydroxide – LDH) $(Cu_{1-x}Zn_x)_{1-y}Al_y(OH)_2(CO_3)_{y/2}\cdot mH_2O$[3] is usually observed as a by-phase after co-precipitation.

In a previous study we have shown that it is possible to obtain Cu-rich (42–49 mol%) phase pure Cu,Zn,Al hydrotalcite by co-precipitation.[4] During calcination two different kinds of material were formed from the single phase precursors – amorphous areas with a Zn : Al ratio of 1 : 2, characteristic for the spinel-like $ZnAl_2O_4$, and granular areas with well crystalline CuO, which are either depleted in Zn or Al (depending on the precursor composition). In the case of a precursor composition approaching the Zn : Al ratio of 1 : 2 little or no segregation was observed during calcination, suggesting the formation of a $CuO/ZnAl_2O_4$-type material in which the spinel phase is X-ray amorphous. Such Cu,Zn,Al hydrotalcites are promising catalyst precursor materials as they show a homogeneous distribution of the metallic and oxidic components and very small Cu particles result after reduction. The main characteristic of these catalysts was that the resulting Cu particles were to a large extent not accessible by the reaction gas, as the particles were strongly embedded into the oxidic matrix. A large Cu surface area is, however, a prerequisite for high catalytic performance of $Cu/ZnO/Al_2O_3$ catalysts.[5] Furthermore, it is known that in addition to a large Cu surface area also intrinsic factors can affect the surface normalized activity of Cu.[5,6] We have recently shown that the embedding of Cu nanoparticles in ZnO/Al_2O_3 may beneficially affect the intrinsic activity of the exposed Cu surface area[7] in methanol synthesis, *i.e.* the activity or concentration of the active sites on the Cu surface. This effect is probably related to the stabilization of a strained and/or defective form of Cu. Lattice strain[8] and planar defects[9] have been identified in previous studies as indicators for high intrinsic activity of the exposed Cu surface area.

The principle of using microemulsions as "nano-reactors" was shown to be a promising approach for the synthesis of nanoparticles in general[10–13] and of Cu-based catalysts in particular.[14] A microemulsion (ME) is defined as a dispersion of two non-miscible liquids, *e.g.* water and oil (typically an organic solvent), and a stabilizing surfactant (more details are given in ESI†). In contrast to classical emulsions, microemulsions are characterized by a small droplet size (5–100 nm) and, hence, belong to colloidal

[a]*Fritz-Haber-Institut der Max-Planck-Gesellschaft, Department of Inorganic Chemistry, Faradayweg 4-6, 14195 Berlin, Germany. E-mail: behrens@fhi-berlin.mpg.de; Fax: +49 30 8413-4405; Tel: +49 30 8413-4408*
[b]*Max-Planck-Institut für Chemische Physik fester Stoffe, Nöthnitzer Str. 40, 01187 Dresden, Germany*

† Electronic supplementary information (ESI) available: More details for the microemulsion technique and the applied system with DLS data, phase diagrams and N_2 physisorption isotherms as well as the determination of interface ratio. See DOI: 10.1039/c2jm16138a

systems. These droplets can be used as confined "nano-reactors". This technique has been utilized to synthesize hydrotalcites[15–17] and was already applied using pH-adjusted microemulsions.[16,18] Herein, we present the ME synthesis of Cu,Zn,Al-LDH by pH-controlled co-precipitation within the ME-droplets using simultaneous dosing of metal salt solution and precipitation agent. Due to the simultaneous addition of all reactants, such synthesis processes can be operated continuously, which allows for easy and feasible up-scaling.

Applying the microemulsion technique to the LDH precursor system is supposed to influence the particle growth during the precipitation process. Furthermore, the present study aims to find a compromise to make small Cu particles more accessible to the reactant gas, but still providing improved interaction with the oxide to maintain stability during reaction and a high intrinsic activity – tested in methanol steam reforming (MSR). The nominal composition was chosen to Cu : Zn : Al = 50 : 17 : 33 as a high content of the active phase is desirable and makes the material comparable to industrially used catalysts. Based on our previous study, the Zn : Al ratio of 1 : 2 should result in materials of a homogeneous $Cu/ZnAl_2O_4$ microstructure.[4]

2 Experimental

2.1 Materials

Inspired by literature reports[11,19,20] the technical non-ionic surfactant Marlipal O13/40 was chosen to apply the microemulsion technique to the synthesis of Cu,Zn,Al-LDH. The surfactant was added to the reaction medium water/cyclohexane. Cyclohexane was supplied by Roth with a purity of 99.9%. Deionized water was taken from a Millipore water treatment system (MilliQ). The used surfactant Marlipal O13/40 ($C_{21}H_{44}O5$) is a non-ionic surfactant of the alkyl polyglycolether type with a mean ethoxylation degree of four and was supplied by Sasol (Marl, Germany) with a purity of 98%. The metal nitrates and bases were supplied by different companies with purities around 99% ($Cu(NO_3)_2$ – Roth, $Zn(NO_3)_2$ – Fluka, $Al(NO_3)_3$ – Riedel-de-Häen, NaOH – Riedel-de-Häen and Na_2CO_3 – by Roth) and were used without further purification.

2.2 Microemulsion synthesis

The water-in-oil microemulsions were prepared by mixing cyclohexane and the surfactant Marlipal O13/40 in a glass flask and adding either water or the salt solution. For the metal salt solutions the microemulsion formed spontaneously by gentle shaking in their stable temperature range (for phase diagrams see ESI†). The base solution needed approximately 12 h until stable microemulsions were formed. Just for practical reasons the microemulsion synthesis of the Cu,Zn,Al-hydrotalcite was carried out with just one microemulsion: A microemulsion ($\gamma = 0.25$, 8% H_2O) of the aqueous solution of NaOH (0.3 M) and Na_2CO_3 (0.045 M) in cyclohexane which was stabilized with the surfactant Marlipal O13/40. The reaction was carried out by adding Cu,Zn,Al nitrate solution and the basic microemulsion at a constant pH value (pH = 8 ± 0.7) at 30 °C – pH and temperature were controlled by an automated lab reactor system (Labmax from Mettler Toledo). A water-in-oil microemulsion without any salts was used as starting template in the vessel. The aqueous $Cu^{2+}/Zn^{2+}/Al^{3+}$ nitrate solution (Cu : Zn : Al = 50 : 17 : 33, total metal concentration: c(M) = 0.43M) was dosed constantly and the basic microemulsion was dosed to maintain the pH. Like this, the hydrotalcite was formed inside the water droplets. This ME synthesis approach can easily be scaled up by implementing a product overflow and running the co-precipitation continuously. Combined with recycling of the organic solvent, a cheap and controlled ME synthesis is possible. The product of the described ME synthesis was isolated by centrifugation, washing with acetone and drying at 100 °C for around 15 h. Upon calcination in air at 330 °C for 3 h the blue-green hydrotalcite was converted into the dark green mixed oxide. A reference catalyst was prepared similar as described by Behrens *et al.*[4] by conventional co-precipitation under analogous conditions – *i.e.* using the same temperature, concentrations and drying as well as calcination procedure afterwards. The precursor samples are labeled "X-LDH", "X" being the short form of the synthesis method – "ME" for the microemulsion sample, "co" for the conventionally co-precipitated sample. The calcined samples are labeled "X-330", where 330 refers to the calcination temperature in °C, and the reduced samples are labeled "X-red".

2.3 Methods

To determine suitable values for γ, α and T, the phase diagrams of all prepared microemulsions were explored by visual observation of the phase boundaries upon gradual change of the temperature (see phase diagrams in ESI Fig. S1†). The dynamic light scattering (DLS) measurements for droplet and particle size distributions were carried out using a Malvern ZetaSizer NS. The average composition of the precipitates was determined by inductively coupled plasma mass spectrometry (ICP-MS). X-ray diffraction (XRD) patterns were recorded on a STOE Stadi-P diffractometer in transmission geometry using Cu-Kα_1 radiation, a primary Ge monochromator and a 3° linear position sensitive detector. The BET surface areas of precursor and calcined samples were determined by measuring the nitrogen adsorption-desorption isotherms with a Quantachrome Autosorb automatic BET-sorptometer at −196 °C with nitrogen as the analysis gas. Prior to the analysis, the samples were outgased for 2 h at 100 °C. IR spectra were collected on a FTIR Perkin Elmer 2000 using the KBr disc technique. Thermogravimetric analyses (TG/DSC) were performed on a Netzsch STA449 thermobalance (2 K min^{-1}, synthetic air). Evolution of the gas phase during reaction was monitored with a quadrupole mass spectrometer (Pfeiffer, QMS200 Omnistar). Calcined samples were reduced in 5 vol% H_2 in Ar at a heating rate of 6 K min^{-1} (80 mL min^{-1}, end temperature 350 °C, holding time 30 min) by a temperature programmed reduction (TPR) in a fixed bed reactor (TPDRO-1100, CE instruments). The H_2 consumption was monitored with a thermal conductivity detector. The copper surface area (Cu SA) of the reduced catalysts was determined in the same machine using N_2O reactive frontal chromatography (N_2O-RFC).[21] N_2O oxidizes the Cu metal surface and is decomposed into O^{2-} and N_2. The experiments were carried out at 30 °C to avoid subsurface oxidation.[22] A stainless-steel micro-reactor was used, which had an inner diameter of 4 mm and was filled with 95 mg of the sieve fraction (100–200 μm). The measurement was started by switching from pure He to 1 vol% N_2O in He (Westfalen) by means of a four

way valve. The amount of evolved N_2 upon decomposition of N_2O at the Cu(0) surface was monitored with a mass spectrometer (Pfeiffer, QMS Omnistar). The Cu surface area is calculated assuming a molar stoichiometry of Cu(s)/N_2 = 2 and a value of 1.46×10^{-19} copper atoms per square meter.[23] SEM images were taken in a Hitachi S-4800 (FEG) system. A Philips CM200FEG microscope operated at 200kV and equipped with a field emission gun and the Gatan imaging filter was used for TEM. The coefficient of spherical aberration was Cs = 1.35 mm. The information limit was better than 0.18nm. High-resolution images with a pixel size of 0.016nm were taken at the magnification of 1'083'000× with a CCD camera, and selected areas were processed to obtain the power spectra (square of the Fourier transform of the image), which were used for measuring interplanar distances (±0.5%) and angles (±0.5°) for phase identification. The catalytic activity was tested in the methanol steam reforming reaction ($CH_3OH + H_2O \rightarrow CO_2 + 3\ H_2$) within a plug-flow reactor system (PID Eng&Tech, $CH_3OH : H_2O = 1 : 1$) using a GC (CP 4900, Varian, columns: molsieve, PPU) for product analysis. The educt gas mixture contained nitrogen as a carrier gas and helium as an internal standard to calibrate the gas volumes, because unconverted water and methanol were removed prior to the GC using a cooling-trap and a Nafion membrane. A sieve fraction of 100–200 μm of the calcined samples was diluted with 200 mg of inert graphite. Both samples were reduced in hydrogen (12 h at 180 °C and 3 h at 260 °C) before starting the steam reforming reaction which was carried out at 260 °C. Conversion of methanol was calculated using the amount of formed carbon oxides. Selectivity of CO_2 was defined as $CO_2/(CO_2 + CO)$ – CO was most likely produced by reverse WGS reaction.

3 Results

3.1 Characterization – LDH precursor and calcined sample

The microemulsion product is characterized in comparison to the co-precipitated one. The average composition of both precursors was determined by ICP-MS and was found to be close to the nominal values (Table 1). Both microemulsion and the conventional co-precipitation result in crystalline materials showing XRD patterns (Fig. 1) which are typical for LDH compounds and match the pattern reported for a sample $Cu_3Zn_3Al_2(OH)_{16}CO_3 \cdot 4H_2O$ (ICSD 37-629).[24] The basal reflections of ME-LDH are clearly broadened, probably due to thinner platelets than in co-LDH. Furthermore, the (00l) reflections are slightly shifted to higher angles and accordingly lower d values result (see Table 1). Such differences could be a consequence of random interstratification, but as the basal series is rational for both materials such random interstratification is not very probable. Furthermore, the observed differences could also result from changes in the interlayer composition (see below). In

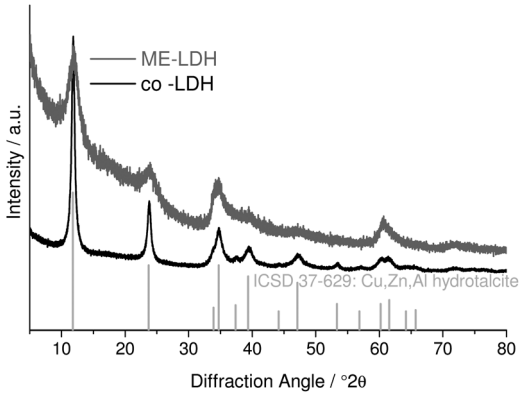

Fig. 1 XRD patterns of reference precursor (co-LDH) and of the product obtained by microemulsion synthesis (ME-LDH).

the SEM images (Fig. 2) it is visible that both products show the typical platelet-like morphology of hydrotalcites, with ME-LDH having a slightly smaller platelet diameter in comparison to co-LDH (see Table 2). The obtained platelets are significant larger than the droplet diameter of the applied microemulsion (see ESI†). This deviance is probably due to growth of the LDH platelets after the microemulsion is destroyed by centrifugation but the precipitate is still in its mother liquor. It has to be mentioned that the influence of applying the microemulsion synthesis on the platelet size is not as large as expected. However, the specific surface area is nearly doubled for ME-LDH (BET in Tab. 2, isotherms are presented in ESI†) whereas the platelet diameter is just slightly decreased. Due to the large aspect ratios of the platelets, the specific surface area is mostly determined by basal surfaces, whereas the edges contribute little. Therefore, reducing the diameter of the platelets has only a minor effect on the specific surface area while reducing the thickness has a dramatic effect. This observation is in agreement with the broader XRD reflections of the basal planes. The thermal behaviour of the catalyst precursor samples was investigated by thermogravimetric measurements in synthetic air coupled with

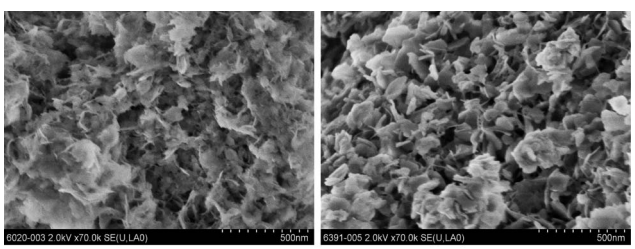

(a) (b)

Fig. 2 SEM images of the precursors: (a) ME-LDH and (b) co-LDH.

Table 1 Metal composition of investigated samples (nominal concentration normalized to the total metal content, values measured by ICP are given in parentheses) and d-values of (00l) reflections of XRD patterns

precursor	mol% Cu	mol% Zn	mol% Al	d(003)/Å	d(006)/Å
ME-LDH	50 (50.3)	17 (16.2)	33 (33.5)	7.44 ± 0.007	3.72 ± 0.004
co-LDH	50 (49.75)	17 (16.15)	33 (34.1)	7.48 ± 0.007	3.74 ± 0.004

Table 2 Lateral particle size of the platelets determined from SEM (100 platelets), BET surface areas measured by N_2 physisorption

	microemulsion			co-precipitation		
state	label	*d*/nm	S_{BET}/m^2g^{-1}	label	*d*/nm	S_{BET}/m^2g^{-1}
precursor	ME-LDH	54	151	co-LDH	64	80
calcined	ME-330	52	128	co-330	59	83

mass spectrometry (TG-MS). In general ME-LDH shows the same features of the thermal behaviour as typical for LDH compounds[25] like co-LDH (Fig. 3): (i) loss of surface water molecules around 70 °C, (ii) evaporation of interlamellar water molecules between 100 °C and 140 °C, (iii) dehydroxylation of the brucite-layer and loss of carbonate of the interlayer space between 140 °C and 220 °C. The last pronounced step of weight loss can be attributed to the well known, strongly bound (so called) high-temperature carbonate (HT-CO_3^{2-})[4,26,27] at 515 °C for ME-LDH and 620 °C for co-LDH respectively. As already claimed elsewhere,[28] a higher decomposition temperature of HT-CO_3^{2-} is an indicator for strong interactions across interfaces and grain boundaries which were formed during the first decomposition step. Accordingly, the lower thermal stability observed for ME-LDH results from a weaker interface contact of the oxidic Cu species with the Zn-Al matrix. The total amount of nitrates is higher in ME-LDH compared to co-LDH, but carbonate was identified as the major anion by XRD (nitrate would give a larger inter-layer spacing[25]) and by comparison of the integrals of the corresponding MS traces (Fig. 3(a)). Additionally, the ME-LDH shows an exothermic event at 230 °C (Fig. 3(a)) which correlates with the formation of CO_2 and H_2O and can be assigned to the combustion of intercalated organic residues, *e.g.* acetone from washing – no indication of adsorbed acetone was found in the MS traces. For ME-LDH the MS signal of the interlamellar water loss at 114 °C exhibits a significant lower intensity compared to the dehydroxylation step. As the weight loss is, furthermore, similar for both samples, organic molecules are assumed to substitute some water molecules in the interlayer of ME-LDH compared to the amount in co-LDH. By IR spectroscopy this is confirmed (see Fig. 4), as the water band of co-LDH at 1650 cm^{-1} is replaced by a vibrational band at 1550 cm^{-1} which is assigned to coordinated carbonyl – probably acetone (used for washing before drying) which remained within the interlayer during the drying process. This is also the most likely explanation for the difference in the interlayer spaces observed by XRD. Furthermore, the other peaks of the spectra (570 cm^{-1} – metal-OH deformation; 1360 cm^{-1}, 840 cm^{-1} – interlayer CO_3^{2-} deformation[29]), all belonging to the LDH compound, show a similar signature for both precursors. All spectra contain a nitrate band at 1385cm^{-1} which results from co-intercalated nitrate anions in the LDH interlayers as well as impurities of the KBr used for dilution.

According to the TG-MS curve, all organic molecules are finally decomposed at 250 °C. As we have shown before, a calcination temperature of 330 °C (for 3 h) is suitable to

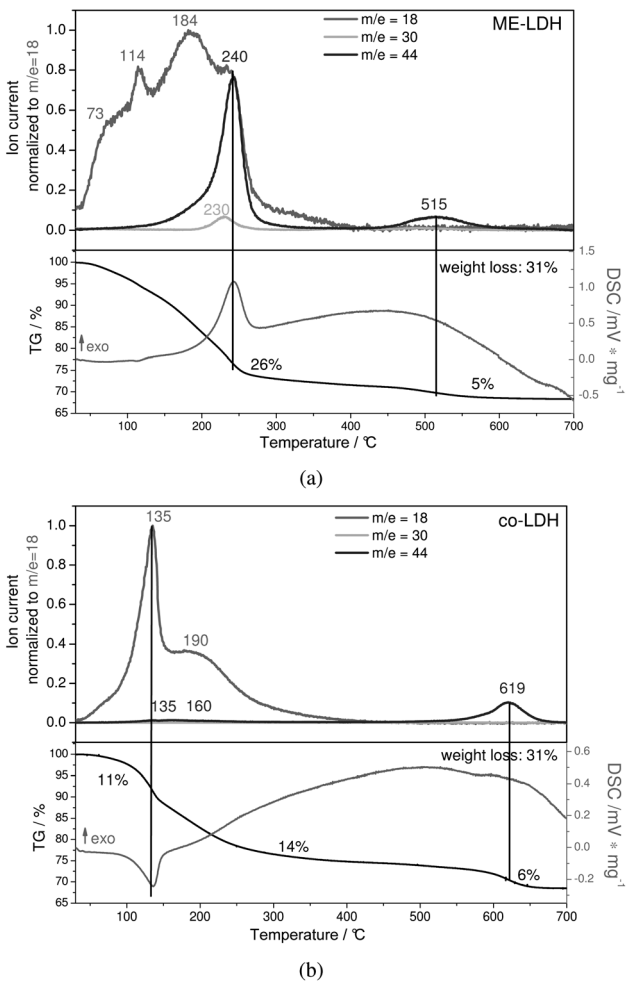

Fig. 3 Weight loss and MS spectra during calcination: (a) ME-LDH and (b) co-LDH; $m/z = 18$ correlating with water evolution, $m/z = 44$ with CO_2 formation and $m/z = 30$ is the NO trace – decomposition product of the nitrates.

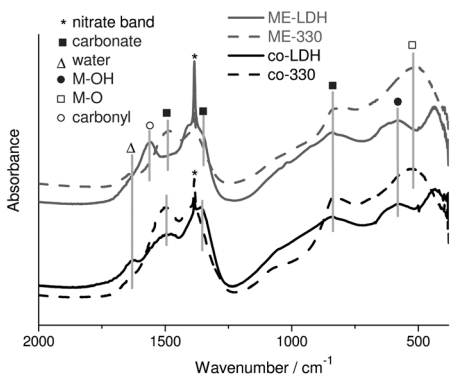

Fig. 4 IR spectra of precursor and calcined samples.

dehydroxylate and decarboxylate the hydrotalcite[4] and is also practicable for the one resulting from microemulsion. During calcination in air at 330 °C both products were converted into nearly amorphous, carbonate containing mixed oxides (Fig. 5) as the oxide phases do not crystallize until the decarbonation step at a temperature above 500 °C.[4] These transformations were also observed by IR spectroscopy (see Fig. 4), where the M–OH band was replaced by the M–O band (510 cm^{-1}) and the carbonate band at 1360 cm^{-1} disappeared, whereas a shoulder at 1480 cm^{-1} remained or evolved in the case of the ME sample which is assigned to HT-CO_3. Furthermore, as the carbonyl band cannot be observed in the IR spectrum of ME-330, all remaining organic is, indeed, decomposed during calcination, as expected from TG-MS. ME-330 still shows the higher BET-SA (see Table 2), but a significant decrease was observed during the calcination process, whereas the platelet diameter (determined by SEM, Table 2) stays nearly constant for both samples. Hence, reduction of the specific surface area during calcination might be caused by an aggregation of the platelets which is supported by an increased inter-particle pore size between the platelets for ME-calc compared to ME-LDH (for details see ESI†). Furthermore, SEM (Fig. 6) revealed that both samples maintained their morphology (Table 2) during calcination, showing again the similarity of the two materials. After calcination to 700 °C a crystalline product results for both samples which only contains CuO and $ZnAl_2O_4$ (see Fig. 7).

3.2 Reduced catalyst

The final Cu/$ZnAl_2O_4$ catalysts, labeled as ME-red and co-red, resulted upon reduction of the Cu component of the calcined samples in hydrogen. The TPR profiles of both samples are depicted in Fig. 8. Both profiles have a similar shape, but the temperature of the maximum reduction rate is significant lower for ME-330, whereas the onset temperature is approximately the same. This observation is an indication for a particle size effect, as ME-330, which is resulting from the calcination of the LDH precursor, exhibits the smaller secondary particles (platy aggregates of CuO nanoparticles and oxide matrix, see platelet diameters in Table 2). The similar shape of the TPR profiles shows the similarity of the Cu phases present in both samples. By calibration using crystalline CuO it is possible to calculate the degree of reduction from the hydrogen consumption (ratio of formed Cu(0) to remaining oxidized Cu). Where co-330 is nearly

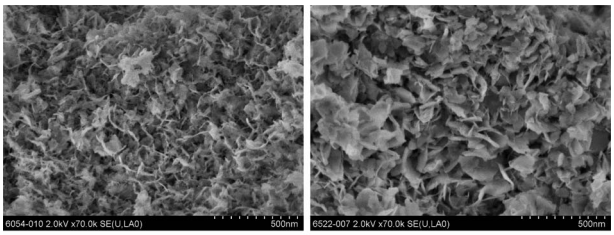

(a) (b)

Fig. 6 SEM images of calcined samples: (a) ME-330 and (b) co-330.

completely reduced (98%), a significant amount of Cu(II) is not reduced for ME-330 (90% reduced). In agreement to our previous study, the TEM images show that the small Cu particles are embedded within the oxide matrix (see Fig. 9). Whereas the Cu particles have a similar size of below 8 nm for both samples (see Table 3 and Fig. 10), the secondary particles (aggregates of Cu nanoparticles and oxide matrix) appear less bulky for ME-red in accordance with the lower platelet thickness of the ME derived sample (see Fig. S6 in ESI†). The Cu surface area of ME-red, is significantly higher (see Table 3) than the one of co-red. Due to the embedding of the Cu particles both catalysts have high interface ratios, *i.e.* the fraction of Cu particles which is not exposed to the gas atmosphere but present as interface to the oxide phase. This value (Table 3) can be calculated from the experimentally measured Cu surface area and the average Cu particle diameter determined by TEM assuming a spherical shape (formulas given in ESI†). In ME-red a higher fraction of the Cu surface is exposed to gas (compare Table 3). Thus, by confining the growth of the LDH precursor particles, the microstructure of the resulting catalyst was modified leading to an increase of the exposed Cu surface area at the expense of interface area.

To compare their catalytic performance both catalysts were measured in methanol steam reforming. The results in Table 4 show a higher activity (hydrogen yield) of ME-red, whereas both catalyst show a similar stability (after 20 h ≈ 69% of the conversion at 2 h) of their performance. The higher activity is attributed to the improved microstructure implied by the application of the ME-technique during precursor preparation. However, the increase of activity of 7% is low in relation to the difference in Cu surface areas of 66%. This result indicates that the intrinsic activity is not constant for a given Cu particle size,

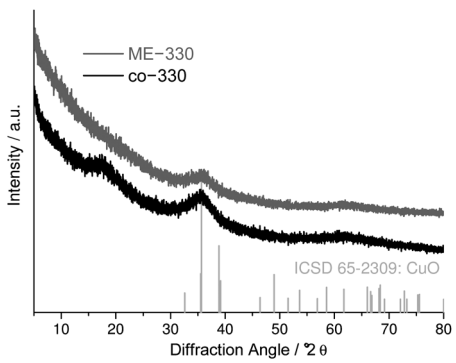

Fig. 5 XRD patterns of samples after calcination: ME-330 and co-330.

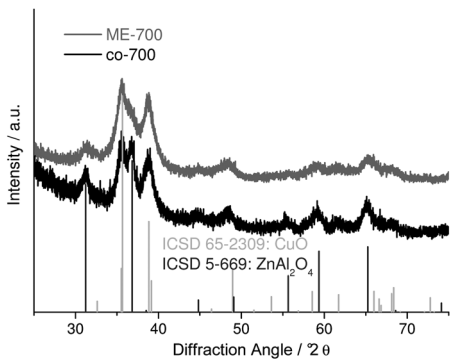

Fig. 7 XRD patterns of samples after calcination in air to 700 °C.

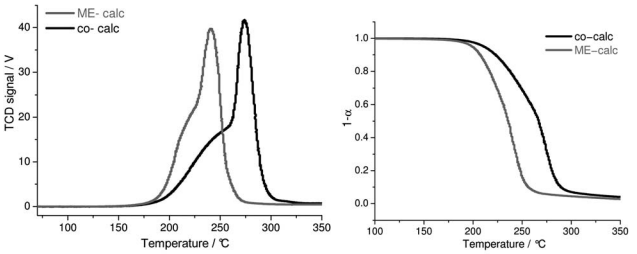

(a) (b)

Fig. 8 TPR of investigated samples: (a) reduction profiles, (b) reduction progress.

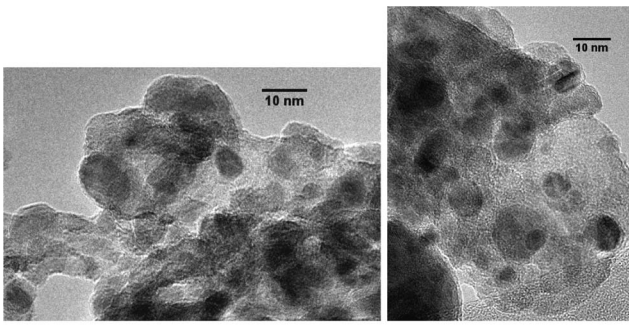

(a) (b)

Fig. 9 TEM images of reduced samples: (a) ME-red and (b) co-red; Cu^0-particles appear as dark spots, while the oxidic Zn-Al-oxide matrix is brighter.

Table 3 Cu particle size measured by TEM (>1000 particles), Cu surface area measured by N_2O-RFC, interface ratio (IFR) and Cu surface area exposed to gas ($Cu\ SA_{exp}$) calculated from TEM images

	d (Cu^0)/nm	Cu SA/m^2g^{-1}	IFR/%	Cu SA_{exp}/%
ME-red	7.8	13.8 ± 1.1	69	31
co-red	7.7	8.3 ± 1.1	83	17

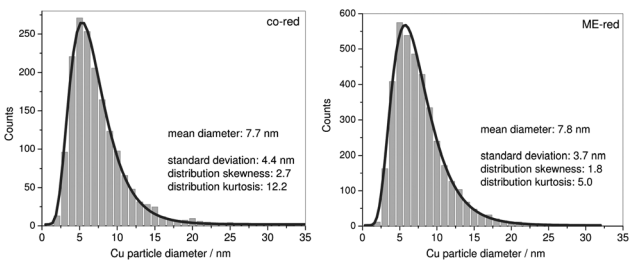

(a) (b)

Fig. 10 Cu particle size distribution after reduction determined from TEM images: (a) ME-red (3863 particles measured) and (b) co-red (1727 particles measured); the average Cu particle sizes are given in Table 3.

but depends heavily on the microstructure of the catalyst. In particular, ME-red exhibits a significantly lower interface ratio than co-red (see Table 3). This is in agreement with the weaker interface interaction which was concluded from the lower decomposition temperature of the high-temperature carbonate.

Table 4 Catalytic properties in methanol steam reforming

	H_2 yield/mmol $g^{-1}h^{-1}$			
	2 h	20 h	X^a/%	S^b/%
ME-red	336.1	232.4	58.8	99.0
co-red	314.8	215.7	63.1	99.5

[a] Conversion compared to feed methanol in % after 20 h on stream. [b] Selectivity to CO_2 in %.

Thus, we assume that the interface interaction with the $ZnAl_2O_4$ matrix seems to beneficially affect the exposed Cu surface. A stabilization of a very active form of non-equilibrium copper has been proposed as the reason for an analogous effect in methanol synthesis.[7] The present study suggests that a similar relation also exists for methanol steam reforming, which is formally the inverse methanol synthesis reaction.

4 Conclusions

We have demonstrated the possibility of applying a pH-controlled co-precipitation for particle synthesis inside the water droplets of a water-in-oil microemulsion. Simultaneous addition of the reactants enables a continuous process and, thus, feasible up-scaling of this synthesis method. We have used this method to synthesize a Cu,Zn,Al hydrotalcite-based catalyst precursor materials. The BET surface area of the ME products (precursor and calcined one) is significantly higher due to thinner precursor platelets than the ones of the conventionally co-precipitated reference catalyst. Accordingly, the ME product exhibits less bulky secondary particles after calcination and reduction, *i.e.* aggregates of CuO or Cu nanoparticles and oxide matrix. The homogeneous distribution of all elements in the precursor state, which was observed for both systems, leads to small Cu particles below 8 nm for both samples. The catalyst resulting from ME exhibits indeed the higher Cu surface area, which is attributed to the smaller size of its $Cu/ZnAl_2O_4$ aggregates and a lower embedding of the Cu particles. Consequently, the ME product exhibits the higher catalytic activity in methanol steam reforming compared to the co-precipitation product. However, the increase in Cu surface area does not scale with the increase in activity. The lower intrinsic activity of the catalyst resulting from micro-emulsion indicates that the Cu surface area is not the only influencing parameter to gain high activity, while effects of Cu particle size could be excluded. In case of the microemulsion product the lower intrinsic catalytic activity is attributed to a weaker interface contact of the Cu phase with the Zn-Al matrix. Interface interactions between Cu and the oxide seem to beneficially affect the activity of the Cu particles and the optimal catalyst requires a compromise of exposed surface and interface.

Acknowledgements

The authors thank Edith Kitzelmann, Gisela Lorenz, Gisela Weinberg as well as Igor Kasatkin for their supporting measurements and Süd-Chemie AG is acknowledged for funding and collaboration.

References

1 R. G. Herman, C. E. Bogdan, P. L. Kumler and D. M. Nuszkowski, *Mater. Chem. Phys.*, 1993, **35**, 233–239.
2 R. H. Höppner, E. B. M. Doesburg and J. J. F. Scholten, *Appl. Catal.*, 1986, **25**, 109–119.
3 F. Cavani, F. Trifiró and A. Vaccari, *Catal. Today*, 1991, **11**, 173–301.
4 M. Behrens, I. Kasatkin, G. Weinberg and S. Kühl, *Chem. Mater.*, 2010, **22**, 386–397.
5 M. Kurtz, N. Bauer, C. Büscher, H. Wilmer, O. Hinrichsen, R. Becker, S. Rabe, K. Merz, M. Driess, R. A. Fischer and M. Muhler, *Catal. Lett.*, 2004, **92**, 49–52.
6 A. Mastalir, B. Frank, A. Szizybalski, H. Soerijanto, A. Deshpande, M. Niederberger, R. Schomücker, R. Schlögl and T. Ressler, *J. Catal.*, 2005, **230**, 464–475.
7 M. Behrens, A. Furche, I. Kasatkin, A. Trunschke, W. Busser, M. Muhler, B. Kniep, R. Fischer and R. Schlögl, *ChemCatChem*, 2010, **2**, 816–818.
8 M. M. Günter, T. Ressler, B. Bems, C. Büscher, T. Genger, O. Hinrichsen, M. Muhler and R. Schlögl, *Catal. Lett.*, 2001, **71**, 37–44.
9 I. Kasatkin, P. Kurr, B. Kniep, A. Trunschke and R. Schlögl, *Angew. Chem.*, 2007, **119**, 7465–7468.
10 B. L. Cushing, V. L. Kolesnichenko and C. J. O'Connor, *Chem. Rev.*, 2004, **104**, 3893–3946.
11 D. Adityawarmana, A. Voigt, P. Veit and K. Sundmacher, *Chem. Eng. Sci.*, 2005, **60**, 3373–3381.
12 D. H. M. Buchold and C. Feldmann, *Adv. Funct. Mater.*, 2008, **18**, 1002–1011.
13 H. Goesmann and C. Feldmann, *Angew. Chem.*, 2010, **122**, 1402–14371.
14 J. Agrell, K. Hasselbo, K. Jansson, S. G. Jöras and M. Boutonnet, *Appl. Catal., A*, 2001, **211**, 239–250.
15 F. Bellezza, A. Cipiciani, U. Costantino, M. Nocchetti and T. Posati, *Eur. J. Inorg. Chem.*, 2009, **10**, 2603–2611.
16 G. Hu and D. O'Hare, *J. Am. Chem. Soc.*, 2005, **127**, 17808–17813.
17 G. Hu, N. Wang, D. O'Hare and J. Davis, *J. Mater. Chem.*, 2007, **17**, 2257–2266.
18 L. Sun, Y. Zhang, J. Zhang, C. Yan, C. Lia and Y. Lu, *Solid State Commun.*, 2002, **124**, 35–38.
19 F. Rauscher, P. Veit and K. Sundmacher, *Colloids Surf., A*, 2005, **254**, 183–191.
20 B. Niemann, F. Rauscher, D. Adityawarman, A. Voigt and K. Sundmacher, *Chem. Eng. Process.*, 2006, **45**, 917–935.
21 G. C. Chinchen, C. M. Hay, H. D. Vandervell and K. C. Waugh, *J. Catal.*, 1987, **103**, 79–86.
22 O. Hinrichsen, T. Genger and M. Muhler, *Chem. Eng. Technol.*, 2000, **23**, 956–959.
23 R. M. Dell, F. S. Stone and P. F. Tiley, *Trans. Faraday Soc.*, 1953, **49**, 195–201.
24 C. Busetto, G. del Piero, G. Manara, F. Trifiro and A. Vaccari, *J. Catal.*, 1984, **85**, 260–266.
25 A. de Roy, *Mol. Cryst. Liq. Cryst. Sci. Technol., Sect. A*, 1998, **311**, 173–193.
26 B. Bems, M. Schur, A. Dassenoy, H. Junkes, D. Herein and R. Schlögl, *Chem.–Eur. J.*, 2003, **9**, 2039–2052.
27 G. J. Millar, I. H. Holm, P. J. R. Uwins and J. Drennan, *J. Chem. Soc., Faraday Trans.*, 1998, **94**, 593–600.
28 M. Behrens, F. Girgsdies, A. Trunschke and R. Schlögl, *Eur. J. Inorg. Chem.*, 2009, **10**, 1347–1357.
29 M. Turco, G. Bagnasco, U. Costantino, F. Marmottini, T. Montanari, G. Ramis and G. Busca, *J. Catal.*, 2004, **228**, 43–55.